PERGAMON

International Journal of Multiphase Flow 27 (2001) 2063–2081

International Journal of Multiphase Flow

www.elsevier.com/locate/ijmulflow

Flow pattern and flow characteristics for counter-current two-phase flow in a vertical round tube with wire-coil inserts

H.Y. Kim [a], S. Koyama [b,*], W. Matsumoto [a]

[a] *Department of Energy and Environmental Engineering, Interdisciplinary Graduate School of Engineering Sciences, Kyushu University, Kasuga, Fukuoka 816-8580, Japan*

[b] *Institute of Advanced Material Study, Kyushu University, Kasuga, Fukuoka 816-8580, Japan*

Received 6 February 2001; received in revised form 2 August 2001

Abstract

Flow pattern, void fraction and slug rise velocity on counter-current two-phase flow in a vertical round tube with wire-coil inserts are experimentally studied. Flow pattern and slug rise velocity are measured visually with a video camera. The void fraction is measured by the quick-closing valve method. Four kinds of coils with different coil pitches and coil diameters are used as inserts. The presence of wire-coil inserts induces disturbance into gas and liquid flows so that the shape and motion of gas slug or bubbles in a wire-coil inserted tube are quite different from those observed in a smooth tube without insert. The bubbly flow occurs in the low gas superficial velocity region in the wire-coil inserted tube, while the slug or churn/annular flow only appears in the smooth tube without insert over the all test range. The measured slug rise velocity in the wire-coil inserted tube is higher than that in the smooth tube. With modified mean flow velocity calculated with core area, the slug rise velocity in wire-coil tube inserted is in good agreement with Nicklin's correlation. The void fraction in a wire-coil inserted tube is lower than that in a smooth tube in the range of high gas superficial velocities. By introducing a simple assumption on considering the effective flowing area, the measured void fractions in a wire-coil inserted tube are in relatively good agreement with the predicted result based on the drift flux model proposed by others with the correlation for slug rise velocity given by others when the coil pitch is dense. © 2001 Elsevier Science Ltd. All rights reserved.

Keywords: Two-phase flow; Wire-coil insert; Counter-current flow; Flow pattern; Void fraction; Slug rise velocity; Vertical tube; Flow visualization; Experiment

* Corresponding author. Tel.: +81-92-583-7831; fax: +81-92-583-7833.
E-mail address: koyama@cm.kyushu-u.ac.jp (S. Koyama).

0301-9322/01/$ - see front matter © 2001 Elsevier Science Ltd. All rights reserved.
PII: S0301-9322(01)00052-0

1. Introduction

The flow pattern and flow characteristics, such as void fraction and slug rise velocity, for counter-current two-phase flow in a vertical smooth tube have been extensively studied for the last few decades. These studies mainly aimed at employing these results to some applications such as bubble column reactor used in the chemical process and cooling systems for nuclear accidents. Recently, for absorption heat pump/refrigeration applications, there has been a new attempt to employ bubble or slug flow absorbers instead of film flow absorbers that have been widely used so far in the industry. Ferreira et al. (1984), Ferreira (1985), Herbine and Perez-Blanco (1995), Merrill and Perez-Blanco (1997), and Merrill et al. (1998) have studied heat and mass transfer performance on the bubble/slug flow absorbers. This attempt was started to solve the poor wettability problem at the film flow absorber operated on the GAX (generator absorber heat exchanger) cycle. The GAX has higher COP than that of conventional ones. (For further study, please refer to the book of Herold et al., 1996.) To embody the GAX cycle, the flow rate ratio, that is defined as the value of the liquid solution flow rate divided by that of the refrigerant flow rate, should be extremely low so that the solution flow rate must be decreased. This results in poor wettability for solution in the film flow absorber. In the bubble/slug flow absorber, the refrigerant in a vapor state generated from the evaporator is supplied into the absorber that is initially filled with the solution liquid, through the vapor distributor located in the bottom of the absorber. Therefore, all parts of the tube wall are wet so that heat and mass transfer performance is expected to be improved. Additionally, finned tubes or tube with the inserts inside are generally used to increase the heat and mass transfer performance by provoking certain turbulences and swirls into a two-phase flow.

With expectation of this heat transfer enhancement effect, in either single or two phase, various types of inserts and internally finned tubes are commonly used for heat exchangers. Webb (1994) presented heat transfer augmentation techniques and enhancement effect with inserts, such as wire-coil and twisted tape. For single-phase flow, an enhancement ratio reaches to nearly 1.30 by employing wire-coil inserts. Recently, Agrawal et al. (1998) studied the heat transfer augmentation by wire-coil inserts during forced convection condensation in a horizontal tube. They used R-22 as a refrigerant. They reported the condensing heat transfer coefficient increase by 100% compared to a smooth tube on a nominal area basis. However, although many studies on heat transfer augmentation by inserts in either a single-phase or a two-phase flow have been performed, most of these studies were done at focusing only enhancement ratio of the heat transfer coefficient. Besides, these studies were performed with pure refrigerant as a working fluid so that no mass transfer takes place. Absorption performance involving coupled heat and mass transfer is greatly affected by liquid–vapor interface characteristics, since the absorption occurs mainly at the liquid–vapor interface and the heat and mass transfer resistance exists on both phases. This resistance is affected by the two-phase flow structure. Consequently, understanding two-phase flow pattern and fundamental flow characteristics in such a tube with inserts is essential to estimate the absorption performance of the bubble/slug absorber.

The earliest theoretical study on the flow pattern for vertical counter-current flow under adiabatic conditions in a smooth tube was made by Taitel and Barnea (1983). Based on theoretical considerations, they suggested several boundaries with regard to transition of flow pattern; bubbly to slug, slug to annular, and flooding boundaries. Yamaguchi and Yamazaki (1982, 1984)

proposed experimental data of flow patterns by visual observation and void fraction for counter-current air–water flow in vertical smooth tubes of diameter $D = 40$ and 80 mm. Yamaguchi and Yamazaki (1984) classified flow patterns into bubbly, slug/semi-annular and annular flows. They proposed a new correlation to predict the void fraction. However, correlation or model regarding the transition limit was not provided. Mishima and Ishii (1984), Mcquillan and Whalley (1985), and Jayanti and Hewitt (1992) among others have proposed slug to churn flow transition models which are originally built on considering a co-current vertical flow. Recently, Ghiaasiaan et al. (1995, 1997) studied the counter-current flow pattern, void fraction and flooding in vertical and inclined smooth tubes using three working fluids with different viscosities. For the basic study to apply bubble/slug flow absorber in the shape of plate-fin heat exchangers, Sohn and Kim (2000) provided flow pattern observation results and void fraction in vertical narrow rectangular channel with air–water working fluid.

Although the two-phase flow patterns and the flow characteristics in a smooth vertical tube have been extensively studied as mentioned above, no study of two-phase flow patterns in vertical tube in the presence of wire-coil inserts was found by the authors, even in the adiabatic two-phase flow, as well as in the flow where absorption occurs.

Prior to analyzing the absorption process, as the first step, this study deals with flow regimes, void fraction and slug rise velocity experimentally for the counter-current two-phase flow with air–water working fluid under the adiabatic condition in both smooth vertical and wire-coil inserted tubes. The objective is to clarify the basic flow characteristics in a wire-coil inserted tube. The experimental results of void fraction and slug rise velocity in wire-coil inserted tube are compared with the previous drift flux model. The modification method to predict void fraction and slug rise velocity in a wire-coil inserted tube is suggested.

2. Experiments

2.1. Experimental apparatus

Fig. 1 shows the schematic diagram of an experimental apparatus used in this study. The experimental rig mainly consists of a water supply line, an air supply line and a visible test tube prepared for observing the flow pattern and measuring void fraction. Water is pumped into two water inlet ports located 500 mm down from the top of the test tube, and divides into two streams after entering into test tube; upward and downward flows. A part of water flows down in the test tube while air bubbles or slugs rise against it. The remaining water stream flows to the top of the test tube, mixed with the air which has risen through the downward water stream. Air is injected into the mixer, located in the bottom of the test tube, through the vertical cylindrically shaped distributor of 20 mm outer diameter having 35 needles of 0.8 mm in inner diameter and 10 mm in length. The water and air supply lines contain two volumetric flowmeters with different measuring ranges. The test tube, including void fraction measuring section, visualization section, and developing section, is made of transparent acrylic tube with 20 mm of inner diameter. The void fraction measuring section is a 500-mm long tube fitted between two quick-closing valves operated by compressed air. The quick-closing valves are normally open and close simultaneously as the compressed air is supplied. The void fraction measuring section

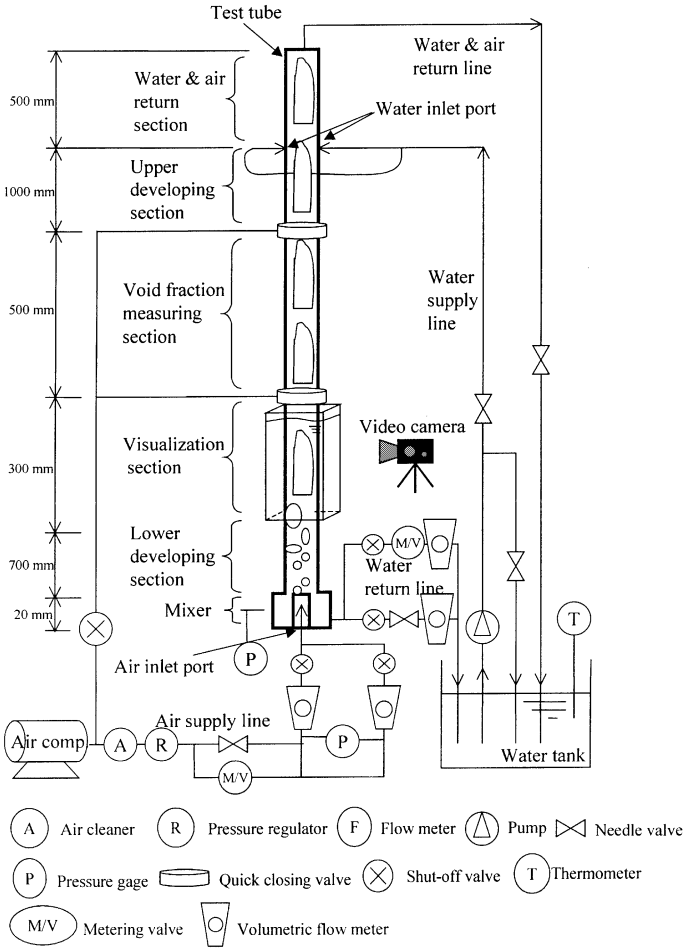

Fig. 1. Schematic diagram of test apparatus.

is located 1000 mm apart from air distributor. The water and air flow rates are controlled manually by needle valves. The flow pattern is observed at the visualization section located just below the void fraction measuring section and recorded by a digital video camera. In order to avoid refraction image, a rectangular water jacket is fitted at outer side of the test tube. Two pressure gages are used. One is for measuring the pressure at the mixer, and the other is for measuring pressure at the air supply line. Two thermometers are inserted at the water tank and ambient air.

The specifications of coils are listed in Table 1 and Fig. 2, where core diameter D_c is defined as

$$D_c = D - 2 \times d. \tag{1}$$

Four kinds of wire-coil inserts, made of stainless steel, with different pitches and/or coil diameters are tested. The experimental range is, approximately, from 0.02 m/s up to flooding occurring in air superficial velocity and 0.005 m/s up to flooding point in water superficial velocity.

Table 1
Specification of wire-coils

Case	Coil		Tube	
	Pitch, P (mm)	Diameter, d (mm)	Core diameter, D_c (mm)	Inner diameter, D (mm)
(a)	15	1	18	20
(b)	15	2	16	
(c)	5	1	18	
(d)	5	2	16	

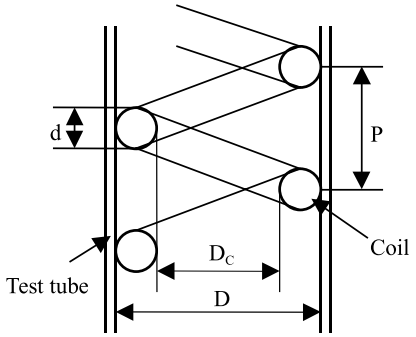

Fig. 2. Geometry of tested wire-coil.

2.2. Experimental procedure

After setting the water and air flow rates to desired values, the flow pattern is observed visually and recorded by the video camera. The void fraction, then, is obtained by measuring the height of trapped water in the test section after two quick-closing valves were closed simultaneously. The data of void fraction are measured *ten times* repeatedly at a randomly selected time on every condition. Ten data are averaged in order to minimize data scattering. The data of temperature and pressure recorded for every test condition are used in calculating the properties of both fluids. The slug rise velocity is obtained by counting the number of frames while one slug travels at the given distance. The slug rise velocity is averaged with randomly chosen five slugs at every test condition to reduce the precision error.

2.3. Uncertainty analysis

Uncertainties of the measuring sensors and error sources are listed in Table 2. Flowmeters, pressure gages and void fraction were calibrated by appropriate methods. Total uncertainty with 95% confidence interval is calculated with the statistical method as

$$U_{0.95} = \sqrt{(B_X)^2 + \left(\frac{t \cdot S_X}{\sqrt{N}}\right)^2}, \tag{2}$$

Table 2
Bios error of sensors and error sources

Item	Accuracy	Full of band	Remarks
Air flowmeter (small)	±0.025 l/min	0.4–5 l/min	From calibration
Air flowmeter (big)	±0.1 l/min	5–50 l/min	From calibration
Water flowmeter (small)	±0.01 l/min	0.1–1 l/min	From calibration
Water flowmeter (big)	±0.1 l/min	1–10 l/min	From calibration
Pressure at flowmeter	±0.01 kg/cm^2	1–5 kg/cm^2	From calibration
Pressure at test section	±0.02 kg/cm^2	1–3 kg/cm^2	From calibration
Water temperature	±0.5 °C	0–100 °C	
Room temperature	±0.5 °C	0–100 °C	
Measured void fraction	±0.2%	0–1	From calibration
Tube diameter	±0.1 mm	20 mm	
Video camera time accuracy	1/30 s		

where B_X is the Bios error, t is the value of Student t distribution, S_X is the standard deviation of the measured data, and N is the number of measurements repeated. Table 3 gives the uncertainties of liquid superficial velocity (U_{LS}), gas superficial velocity (U_{GS}), void fraction and slug rise velocity with typical cases of test data in the smooth tube. Note that +ve of U_{LS} and U_{GS} signify liquid flowing towards downward direction and gas flowing in the upward direction, respectively. The uncertainty values of the void fraction are within the range of ±0.06. The uncertainties of slug rise velocities obtained from video images are within ±0.09 m/s.

Table 3
Uncertainties of data

Case	Item	Value	Bios uncertainty	Precision uncertainty	Total uncertainty	Relative uncertainty (%)
1	U_{LS} (m/s)	0.0049	5.33e − 4	–	5.33e − 4	10.8
	U_{GS} (m/s)	0.021	1.6e − 3	–	1.6e − 3	7.5
	Void fraction	0.2	0.002	0.0286	0.0287	14.7
	Slug velocity (m/s)	0.188	0.0059	0.0085	0.0104	5.5
2	U_{LS} (m/s)	0.0049	5.33e − 4	–	5.33e − 4	10.8
	U_{GS} (m/s)	1.06	1.38e − 2	–	1.38e − 2	1.3
	Void fraction	0.78	0.002	0.0569	0.0569	7.26
	Slug velocity (m/s)	0.86	0.12	0.10	0.16	18.6
3	U_{LS} (m/s)	0.105	5.41e − 3	–	5.41e − 3	5.1
	U_{GS} (m/s)	0.021	1.35e − 3	–	1.35e − 3	6.4
	Void fraction	0.3	0.002	0.063	0.063	21.2
	Slug velocity (m/s)	0.074	0.0009	0.0066	0.0066	9.0
4	U_{LS} (m/s)	0.105	5.41e − 3	–	5.41e − 3	5.1
	U_{GS} (m/s)	1.06	1.41e − 2	–	1.41e − 2	1.3
	Void fraction	0.84	0.002	0.0362	0.0363	4.32
	Slug velocity (m/s)	0.6	0.06	0.069	0.092	15.3

3. Results and discussion

3.1. Flow pattern visualization

In this study, the flow regimes are classified into three categories: bubbly, slug and churn/annular flows. The bubbly flow regime is defined where relatively small bubbles compared with the tube diameter rise over all the test tube. In the slug flow regime, the small bubbles are observed near the gas distributor and developed into gas slug by coalescence of the bubbles. This formed gas slug rises in stable, up to water inlet port of the test tube. The churn/annular flow regime is mainly an annular flow over all the test tube, however, occasionally flooding type waves form from the bottom and move upwards to the top of the test tube. This type of flow was already reported by Ghiaasiaan et al. (1995). The typical flow patterns observed in the tube with wire-coil insert of case (a) ($P = 15$ mm and $d = 1$ mm) are shown in Fig. 3, where Figs. 3(a), (b), and (c) correspond to bubbly flow, slug flow, and churn/annular flow, respectively.

Fig. 4 shows the gas bubble or slug motion at $Q_L = 0.1$ l/min and $Q_G = 1.0$ l/min which corresponds to $U_{GS} = 0.06$ m/s and $U_{LS} = 0.005$ m/s, respectively, with various coils as described in Table 1. It is confirmed from photographs that a number of small bubbles rise in cases (a) and (b) while well-shaped Taylor bubbles rise in smooth tube and case (d) ($P = 5$ mm, $d = 2$ mm). Although the flow in case (c) seems to be slug flow, the shape of gas slug is quite distorted and the gas slug rotates in the radial direction due to presence of wire-coil. In the flow of case (d), a gas slug is longer than that in a smooth tube under identical gas and liquid flow rate conditions.

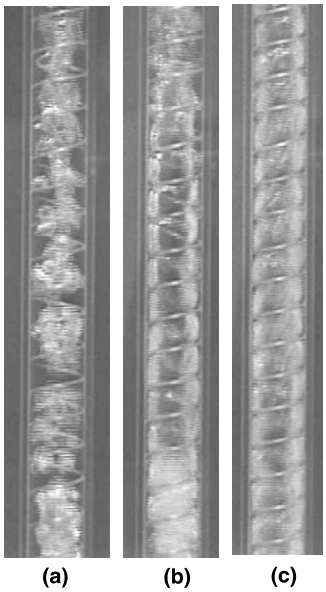

Fig. 3. Observed flow patterns in a tube: (a) bubbly flow; (b) slug flow; (c) churn/annular flow.

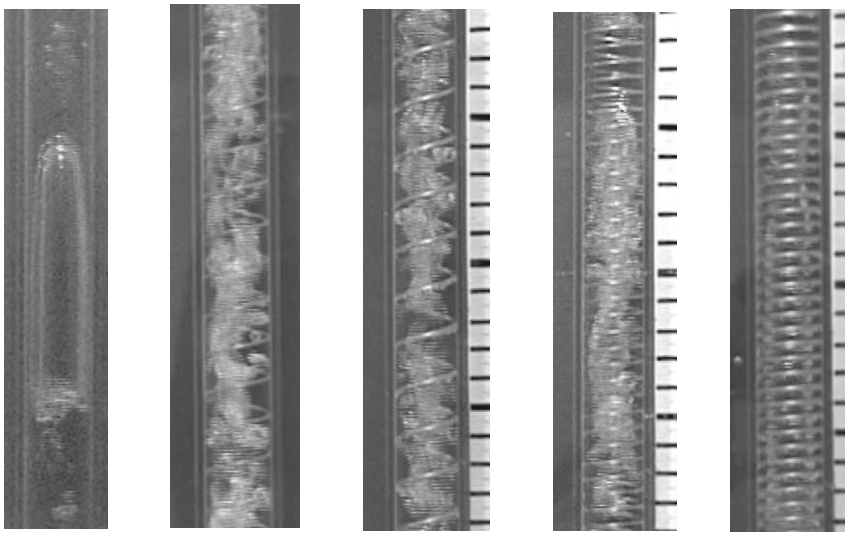

Fig. 4. Visualization of flow motion.

3.2. Flow pattern in smooth tube

Fig. 5 shows the observed flow pattern in the smooth vertical tube, on the map of gas superficial velocity U_{GS} and liquid superficial velocity U_{LS}. The lines signify previous transition limitations given by Taitel and Barnea (1983) and Ghiaasiaan et al. (1995). Taitel and Barnea (1983) sug-

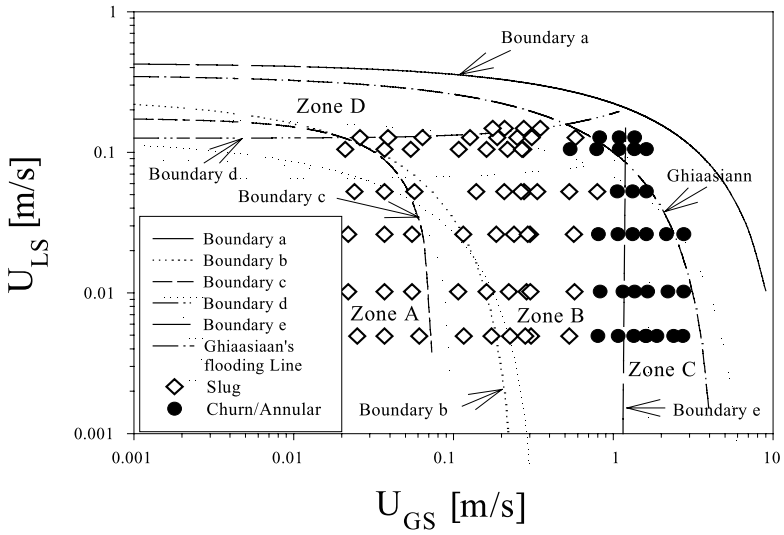

Fig. 5. Flow pattern map for counter-current flow in smooth tube.

gested boundaries a, b, c, d, and e to divide the flow pattern region. The boundaries b and c are transition boundaries from bubbly flow to slug flow that are given as

$$U_{LS} = U_{GS} + U_0 - \sqrt{4U_{GS}U_0} \text{ (boundary b)}, \tag{3}$$

$$0.3U_{LS} + 0.7U_{GS} = 0.21U_0 \text{ (boundary c)}, \tag{4}$$

where U_0 signifies the rise velocity of large bubbles given by Harmathy (1960) as

$$U_0 = 1.53\left[\frac{g\Delta\rho\sigma}{\rho_L^2}\right]^{1/4}. \tag{5}$$

The transition boundary from slug to annular flow (boundary d) is given as

$$U_{LS} = 4\frac{\delta}{D}U_f, \tag{6}$$

where U_f represents the downward velocity of film between the gas slug and wall and δ represents the film thickness. To obtain these values, the following two equations are solved by iteration:

$$\frac{\delta}{D} = B\left[\frac{\mu_L^2}{D^3 g\Delta\rho\rho_L}\right]^p\left[\frac{4\rho_L U_f D}{\mu_L}\right]^q, \tag{7}$$

$$U_{GS} - U_{LS} = \frac{4(\delta/D)U_f - 0.35\sqrt{gD}(1-4(\delta/D))}{0.2 - 4.8(\delta/D)}, \tag{8}$$

where B, p, and q are equal to 0.00448, 5/6 and 3/2, respectively, for turbulent flow. For laminar flow, these values are 0.8667, 1/2 and 1/2. The other transition limit from slug to annular flow (boundary e) when gas flow rate increases is given as

$$U_{GS} - U_{LS} = \frac{\left\{C[gD\Delta\rho]^{1/4} - \left[4(\delta/D)U_f\rho_L^{1/2}\right]^{1/2}\right\}^2}{1.2(1-4(\delta/D))\rho_G^{1/2}} - 0.292\sqrt{gD}. \tag{9}$$

The boundary a, related to flooding limitation, was given by Wallis (1969) based on the experimental data as

$$\sqrt{U_{GS}\sqrt{\frac{\rho_G}{gD(\rho_L-\rho_G)}}} + m\sqrt{U_{LS}\sqrt{\frac{\rho_L}{gD(\rho_L-\rho_G)}}} = C, \tag{10}$$

where m and C are the constants depending on channel end condition. For the turbulent flow, $m = 1$ and $C = 0.88$–1 have been reported by Wallis (1969). The boundary a is drawn with $C = 1$ and $m = 1$. Ghiaasiaan et al. (1995) suggested that C and m, in their test facility that has a similar structure used for our study, are 0.6 and 0.66, respectively. The symbols in Fig. 5 signify experimental data observed in this study. The bubbly flow is unable to be observed. In vertical countercurrent two-phase flow, it is known that bubbly and slug flow patterns are not unique under given conditions. One among bubbly, slug or annular flow possibly exists at the Zone A in Fig. 5. Similarly, slug or annular flow can exist at Zone B. In the Zones C and D, only annular flow can exist. The flow pattern actually taking place under given conditions depends on initial operating conditions and gas or liquid inlet geometry, etc. The slug to churn/annular flow transition

boundary was observed at a slightly lower gas superficial velocity than boundary e. Above boundary d, air slug is unable to rise against water flowing down. The flooding data, which are the symbols located at the most outside in the map, disagree with boundary a. Instead, the test data agree relatively well with the flooding line drawn by Eq. (10) with $m = 0.66$ and $C = 0.6$, which are used by Ghiaasiaan et al. (1995), except in the range of high liquid superficial velocities. The flooding occurs at a higher gas superficial velocity than Ghiaasiaan's flooding line when liquid superficial velocity is higher than approximately 0.1 m/s.

3.3. Void fraction in smooth tube

The void fraction α in smooth tube is shown in Fig. 6. Experimental data are compared with drift flux model proposed by Wallis (1969), which has been commonly used for explaining the bubbly and slug two-phase flow behaviors inside tube or channel regardless of liquid flow direction. The void fraction in this model is calculated as

$$\alpha = \frac{U_{GS}}{C_0 U_m + V_{Gj}}, \tag{11}$$

where U_m is the mean flow velocity defined as $U_m = U_{GS} - U_{LS}$ and C_0 is a two-phase distribution parameter for a round tube given as

$$C_0 = 1.2 - 0.2\sqrt{\frac{\rho_G}{\rho_L}} \tag{12}$$

and the gas drift flux correspond to Taylor bubble velocity rising in a stationary liquid given by Nicklin et al. (1962) as

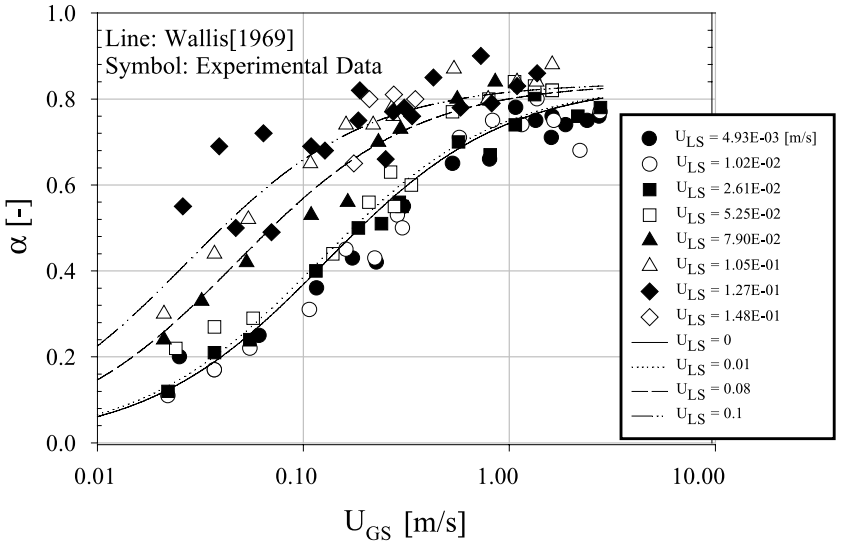

Fig. 6. Measured void fraction in a smooth tube.

$$V_{Gj} = U_{B,\infty} = 0.35\sqrt{\frac{g\Delta\rho D}{\rho_L}}. \tag{13}$$

In Fig. 6, the symbols of open circle, close triangle and open triangle nearly correspond to dotted line, dashed line, and dot–dot–dash line, respectively. The void fraction data are in good agreement with the line calculated by the drift flux model combined with Nicklin's slug rise velocity. For the convenience of comparison between the test data and the drift flux model, Fig. 7 shows the relation between U_{GS}/α and the mean flow velocity, U_m. The symbols represent test data all over the test range of U_{LS} and U_{GS}. The solid line is the calculated value with modified coefficient C_0 and $U_{B,\infty}$ proposed by Usui (1989) based on his test data (downward co-current flow), which is given as

$$C_0 = 1.2 - \left(2.95 + 350E_0^{-1.3}\right)^{-1}, \tag{14}$$

$$U_{B,\infty} = C_1\sqrt{\frac{g\Delta\rho D}{\rho_L}}, \tag{15}$$

where $C_1 = 0.345(1 - \frac{e^{3.37-E_0}}{10})$ and E_0 is the Eötvös number defined as

$$E_0 = \frac{g\Delta\rho D^2}{\sigma}. \tag{16}$$

All experimental data are well fitted with the drift flux model with Nicklin's slug velocity correlation while Usui's model underestimates U_{GS}/α compared with the present data.

Fig. 8 shows the slug rise velocity U_B measured from outside of the test tube while liquid flows down, versus mean flow velocity U_m. Note that Nicklin's slug rise velocity (Eq. (13)) is available when gas slug rises in the stationary liquid. When the liquid flows, Eq. (13) is replaced by

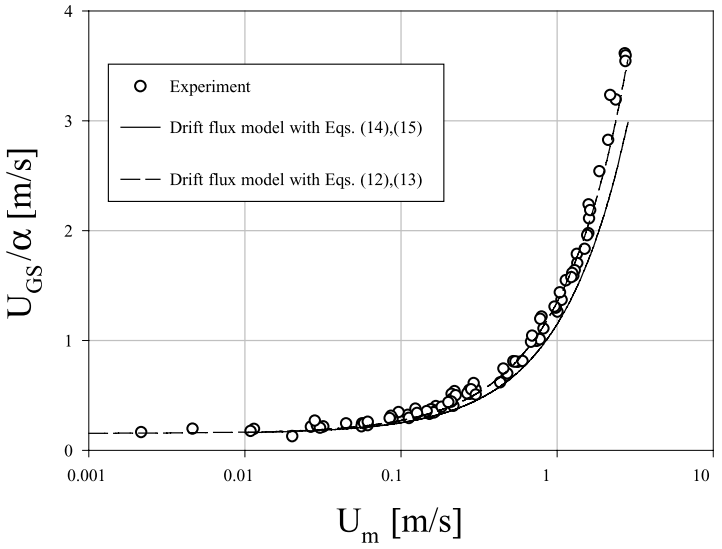

Fig. 7. U_{GS}/α versus mean flow velocity based on the drift flux model.

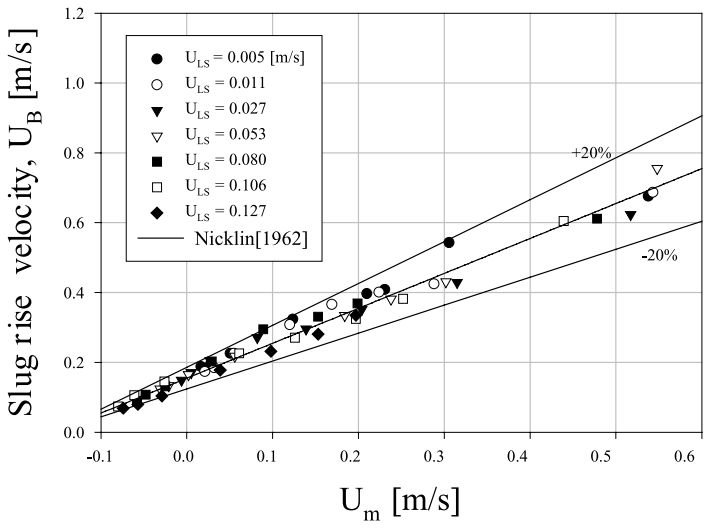

Fig. 8. Slug rise velocity in a smooth tube.

$$U_B = U_m + U_{B,\infty}. \tag{17}$$

The measured slug rise velocities are in good agreement with Eq. (13) within ±20% in Fig. 8.

3.4. Flow pattern in wire-coil inserted tube

The two-phase flow pattern in a wire-coil inserted tube is shown in Figs. 9(a)–(d), which correspond to cases (a)–(d) in Table 1, respectively. Both U_{GS} and U_{LS} were calculated with the cross-sectional area of tube without a wire-coil insert. As shown in Figs. 9(a)–(c), the bubbly flow is observed, while the flow pattern does not appear in a smooth tube. This phenomenon can be explained by the fact that the wire-coil insert induces flow disturbance into liquid flow, which leads to prevent the tendency of wall peaking of bubbles in bubbly flow. Consequently, the coalescence of small bubbles is suppressed in a wire-coil inserted tube. For case (d), however, bubbly flow is not observed similar to the case of a smooth tube. It is interpreted that the coil is so dense in the flow direction that liquid and gas flow smoothly in the core area, and the space between neighboring coils is filled with the re-circulating liquid. The slug to churn/annular flow transition along with the gas superficial velocity, U_{GS}, in the wire-coiled tube appears at lower U_{GS} than that in a smooth tube. This trend is apparently shown in cases (b) and (d), which have coils of 2 mm in diameter. The flooding in cases (b)–(d) occurs at smaller U_{GS} and U_{LS} than Ghiaasiaan's flooding line or boundary d.

Note that these superficial velocities, U_{GS} and U_{LS}, were calculated with the cross-sectional area of the tube alone. Therefore, the actual flowing cross-sectional area when the wire-coil insert exists should require some modifications. Assuming that the actual passage area in a wire-coiled tube is inner area excluding the space blocked by wire-coil in the flow direction, the corresponding diameter D_c can be introduced and, therefore, the corresponding cross-sectional area of wire-coil

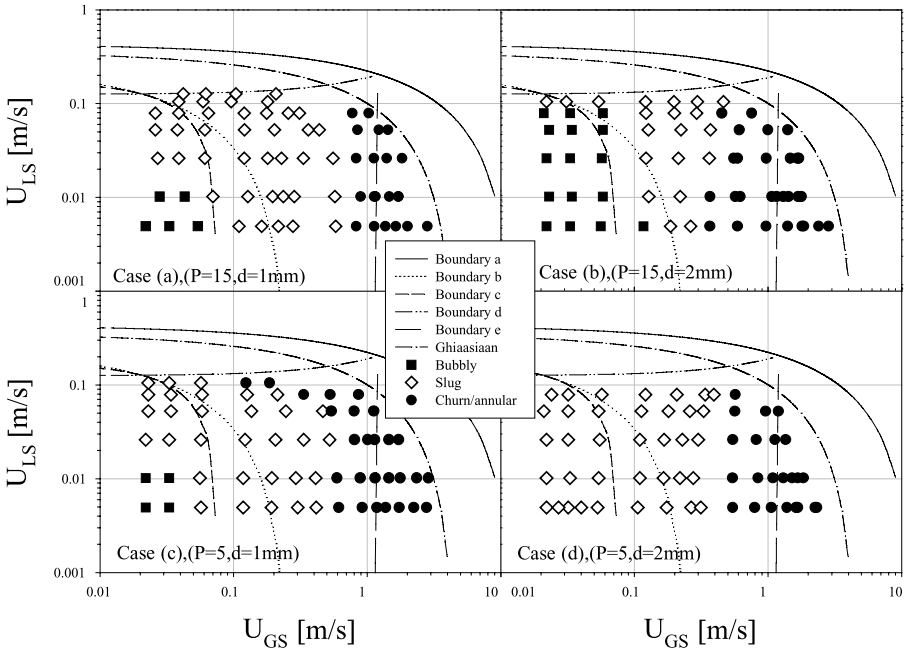

Fig. 9. Flow pattern map in a wire-coil inserted tube.

inserted tube is $A_c = \pi D_c^2/4$. $U_{GS,modified}$ and $U_{LS,modified}$ were calculated based on the above corresponding area are

$$U_{GS,modified} = \frac{Q_G}{A_c}, \tag{18}$$

$$U_{LS,modified} = \frac{Q_L}{A_c}, \tag{19}$$

where Q_G and Q_L signify the gas and liquid volumetric flow rates, respectively. Fig. 10 shows the flow patterns in the wire-coil inserted tube with respect to $U_{GS,modified}$ and $U_{LS,modified}$. The boundaries of each flow pattern of experimental data agree better with the boundary lines proposed by Taitel and Barnea (1983) and the flooding line given by Ghiaasiaan et al. (1995). However, in cases (a) and (b) ($P = 15$ mm), flooding occurs at a higher gas superficial velocity than in Ghiaasiaan's flooding line that was in fair agreement with the test data in a smooth tube. This implies that the flow behavior in a wire-coil inserted tube, especially in case that pitch is large, is not similar to that in a smooth tube. Therefore, correction is required in the assumptions described above.

3.5. Slug rise velocity and void fraction in wire-coil inserted tubes

The measured value of slug rise velocity U_B with U_m in the wire-coil inserted tubes is plotted in Fig. 11. Note that the slug rise velocity is obtained only in the slug flow regime. The slug rise velocities in a wire-coil inserted tube are apparently higher than by Nicklin's correlation. With the

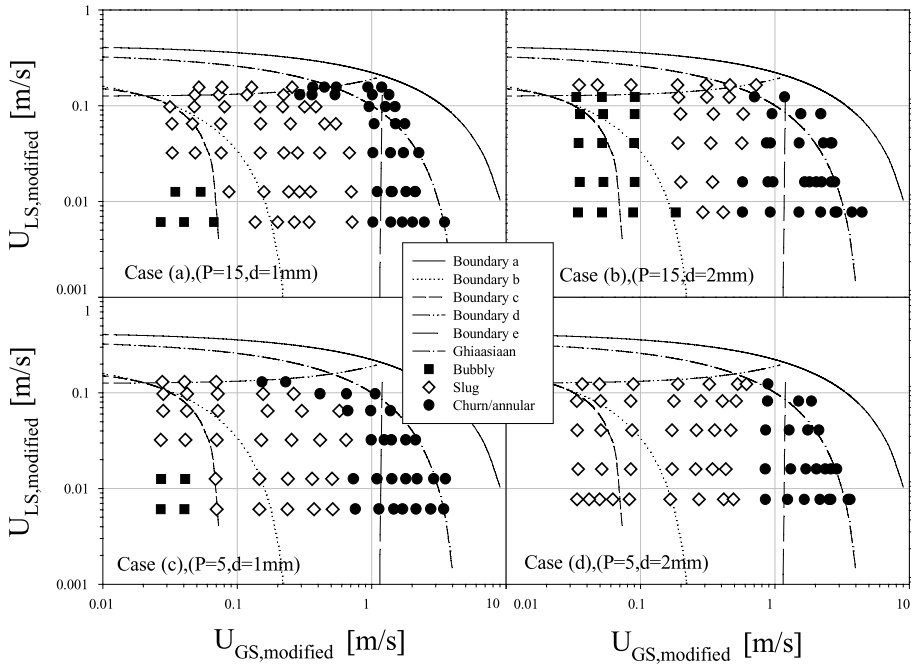

Fig. 10. Modified flow pattern map in a wire-coil inserted tube.

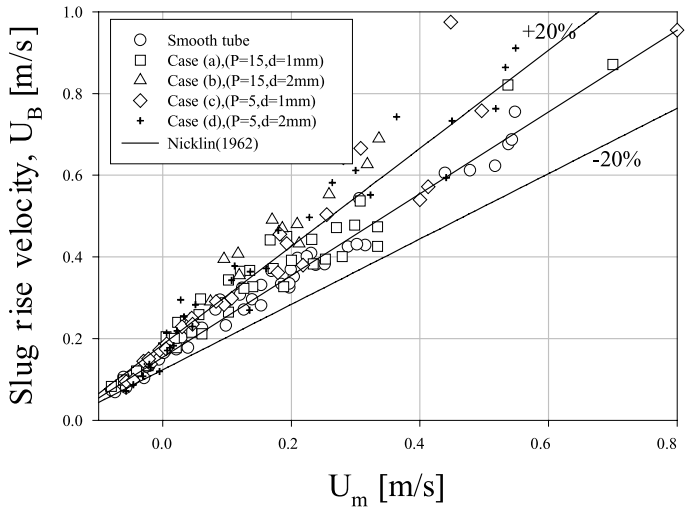

Fig. 11. Slug rise velocity with mean flow velocity.

same method used in the modifying superficial velocity as described above, modified mean flow velocity, $U_{\mathrm{m,modified}}$, is defined as

$$U_{\mathrm{m,modified}} = U_{\mathrm{GS,modified}} - U_{\mathrm{LS,modified}}. \tag{20}$$

Fig. 12 shows the slug rise velocity versus $U_{m,modified}$, with all kinds of coils used in the present study. Most of the test data agree with Nicklin's equation within ±20%.

The void fractions in a wire-coil inserted tube are plotted in Fig. 13. The void fraction in a wire-coil inserted tube is much lower in the range of high gas superficial velocities than that in a smooth

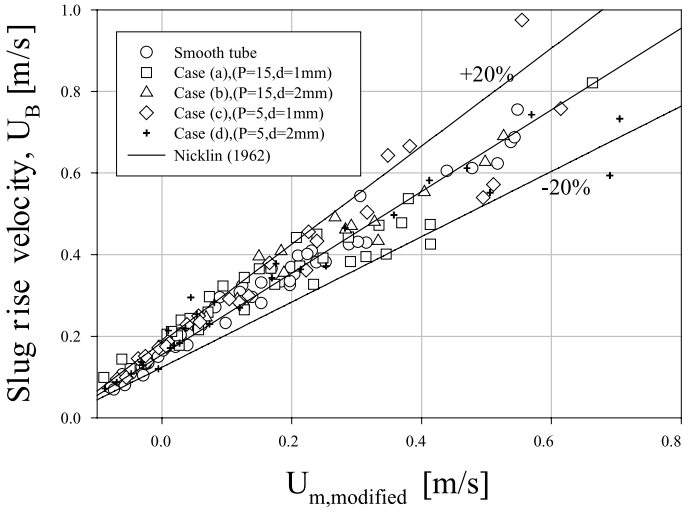

Fig. 12. Slug rise velocity with modified mean flow velocity.

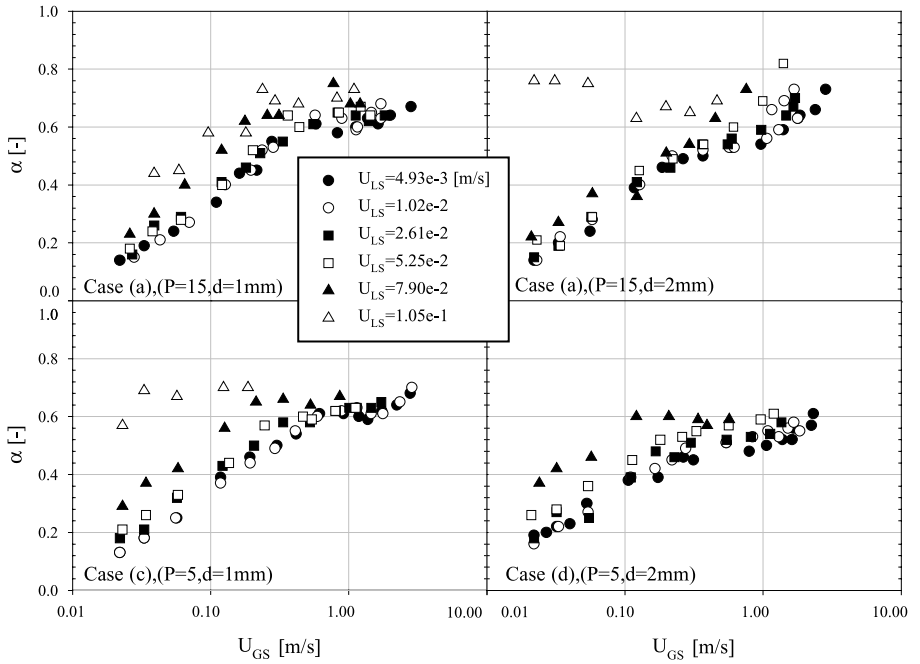

Fig. 13. Measured void fraction in a wire-coil inserted tube.

tube, as shown in Fig. 6 at the same U_{GS} and U_{LS}. This result implies that the water film thickness is thicker and/or the certain amount of water is trapped in the space between neighboring coils near the tube wall, especially when the gas superficial velocity is high. The value of U_{GS}/α with U_m in both smooth and wire-coil inserted tubes is shown in Fig. 14. The value of U_{GS}/α in the wire-coil inserted tube is higher than that of smooth tube and the drift flux model with Nicklin's slug velocity. This is caused by the lower measured void fraction in a wire-coil inserted tube than in a smooth tube.

Consider the configuration geometry of a wire-coil inserted tube, as shown in Fig. 15. Assuming gas flows only in the core area, the modified void fraction can be expressed as

$$\alpha_{\text{modified}} = \frac{V_g}{V_{l,in} + V_g} = \alpha_{\text{measured}}(1 + \beta), \tag{21}$$

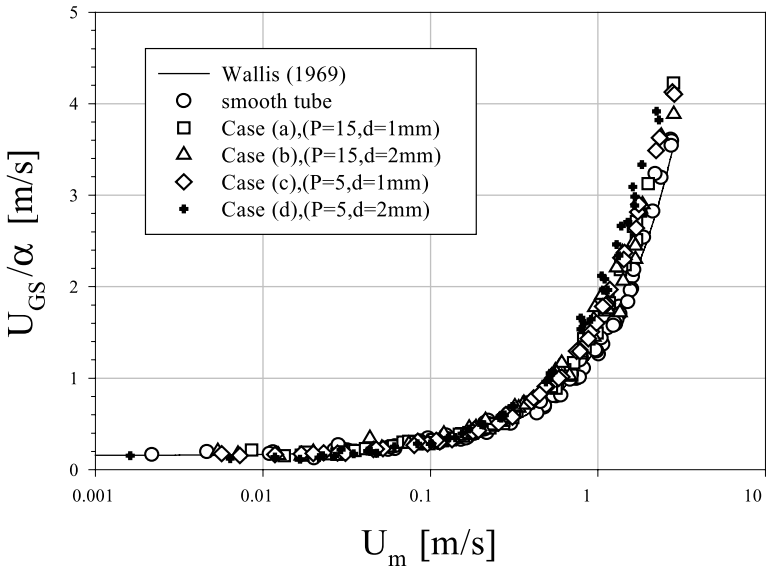

Fig. 14. Comparison between test data in wire-coil inserted tube and drift flux model.

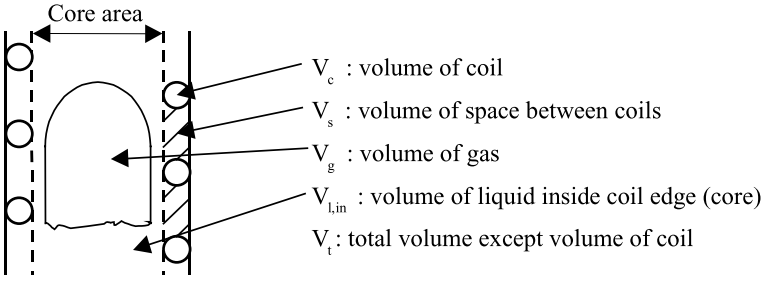

Fig. 15. Geometrical consideration of test tube with wire-coil inserts.

where

$$\beta = \frac{V_s}{V_g + V_{l,in}}, \tag{22}$$

$$\alpha_{measured} = \frac{V_g}{V_t}, \tag{23}$$

$$V_t = V_g + V_s + V_{l,in}, \tag{24}$$

where $\alpha_{measured}$ denotes the measured void fraction in the test and V represents the volume of the part in the wire-coil inserted tube, as shown in Fig. 15. Fig. 16 shows the relationship between $U_{GS,modified}/\alpha_{modified}$ and $U_{m,modified}$. Solid line is drawn from the drift flux model. All the data show a good agreement with the drift flux model except data for case (b), at which $P = 15$ mm and $d = 2$ mm. The reason why the data in case (c) do not agree with the drift flux model is that some portion of the gas slug flows outside the core area. It is able to be found in the visualization image

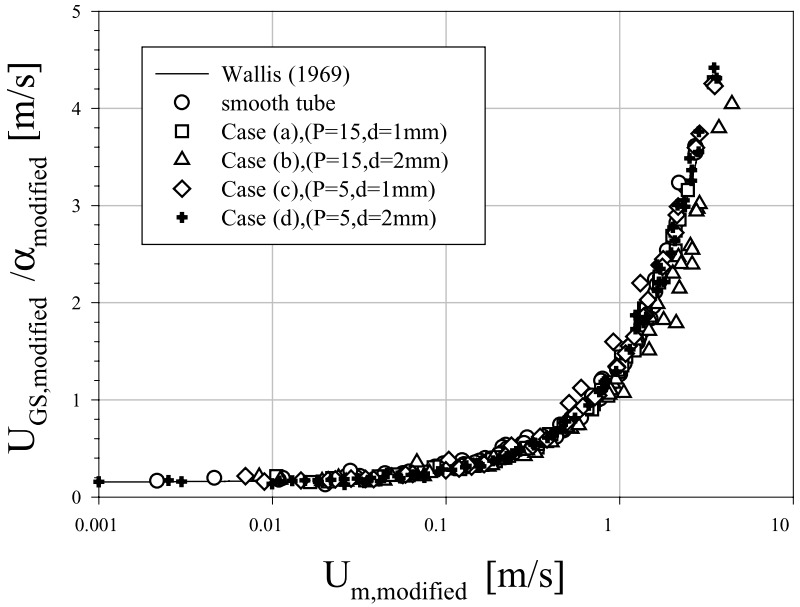

Fig. 16. Comparison between modified data and drift flux model.

Table 4
Values of non-dimensional geometrical parameter

Case	P/D	d/D
(a)	0.75	0.05
(b)	0.75	0.1
(c)	0.25	0.05
(d)	0.25	0.1

that rising gas slugs or bubbles do not flow only the inside core area but also inside neighboring coils along the tube wall.

The values of parameters P/D and d/D with all used coils are given in Table 4. Generally, the modification employed in Eq. (21) is valid when P/D is small. Therefore, Eq. (21) is acceptable when P/D is smaller than 0.25 when the d/D is either 0.05 or 0.1. The modification factor β in Eq. (22) approaches to zero and a_{modified} in Eq. (21) approaches to a_{measured} as the value of d/D decreases. In other words, the void fraction in a wire-coil inserted tube calculated by Eq. (21) approaches to the void fraction in a smooth tube with decreasing the coil diameter. Therefore, Eq. (21) is available to the extent of $d = 0$. This signifies a smooth tube case. Considering the cases when P/D is 0.75 (cases (a) and (b)), Eq. (21) is only available when the parameter d/D is smaller than 0.05. As a conclusion, Eq. (21) is available in the following ranges:

$$0 \leqslant d/D \leqslant 0.1 \quad \text{for } 0 \leqslant P/D \leqslant 0.25, \tag{25}$$

$$0 \leqslant d/D \leqslant 0.05 \quad \text{for } 0.25 \leqslant P/D \leqslant 0.75. \tag{26}$$

4. Conclusions

A study on the flow pattern, the void fraction and the slug rise velocity for the counter-current two-phase flow in a vertical round tube with or without wire-coil insert has been performed. The inner diameter of the test tube is 20 mm and the total length is 3000 mm. Four kinds of wire-coil inserts with different pitches and coil diameters were tested. The experimental range is from 0.02 m/s in U_{GS} and 0.005 m/s in U_{LS} to flooding occurring.

The data of flooding in the smooth tube are in relatively good agreement with flooding correlation with coefficient $C = 0.6$ and $m = 0.66$ proposed by Ghiaasiaan et al. (1995), except high liquid superficial velocity region. The slug to churn/annular transition in smooth tube takes place at lower U_{GS} than boundary e given by Taitel and Barnea (1983). The slug and churn/annular flows only appear in a smooth tube while the bubbly flow appears in a wire-coil inserted tube of cases (a)–(c) in the low U_{GS} region. The flow pattern transition from slug flow to churn/annular flow and flooding in wire-coil inserted tube occur at lower gas superficial velocity than that in a smooth tube. However, by introducing modified superficial velocity calculated with corresponding core diameter D_{c}, on the assumption that gas flows only in core area, the flooding and the slug to churn/annular transition data plotted with modified superficial velocity in the wire-coil inserted tube are similar to the result in a smooth tube without insert.

The measured void fraction in the smooth tube agrees well with the calculated value by using the drift flux model with Nicklin's slug rise velocity. The void fraction in wire-coil inserted tubes are apparently lower than that in a smooth tube at equal liquid and gas flow rates. This resulted from re-circulating liquid in the space between neighboring coils and/or thick liquid film. The void fraction modified on the assumption that liquid fills the space between neighboring coils and gas flows only in the core area is in good agreement with the drift flux model only except case (b) of which $P = 15$ mm and $d = 2$ mm. Most of the slug rise velocities obtained in the slug flow regime, with modified mean flow velocity $U_{\text{m,modified}}$ in wire-coil inserted tubes agree with Nicklin's correlation within $\pm 20\%$.

The present results will give fundamental knowledge in developing a model for absorption process. Those data, such as flow pattern, void fraction and slug rise velocity, provide information for estimation of the film thickness, gas slug velocity, liquid film velocity, and relative velocity at the interface. Furthermore, the authors could confirm that the drift flux model with modification can be available for the two-phase flow in wire-coil inserted tube. The authors believe that this experimental data will facilitate to design a compact absorption system.

References

Agrawal, K.N., Anil Kumar, M.A., Behabadi, A., Varma, H.K., 1998. Heat transfer augmentation by coiled wire inserts during forced convection condensation of R-22 inside horizontal tubes. Int. J. Multiphase Flow 24, 635–650.

Ferreira, C.A., Keizer, C., Machielsen, C.H.M., 1984. Heat and mass transfer in vertical tubular bubble absorbers for ammonia–water absorption refrigeration systems. Int. J. Refrig. 7, 348–357.

Ferreira, C.A., 1985. Combined momentum, heat and mass transfer in vertical slug flow absorbers. Int. J. Refrig. 8, 326–334.

Ghiaasiaan, S.M., Taylor, K.E., Kamboj, B.K., Abdel-khalik, S.I., 1995. Countercurrent two-phase flow regimes and void fraction in vertical and inclined channels. Nucl. Sci. Eng. 119, 182–194.

Ghiaasiaan, S.M., Wu, X., Sadowski, D.L., Abdel-khalik, S.I., 1997. Hydrodynamic characteristics of counter-current two-phase flow in vertical and inclined channels: effects of liquid properties. Int. J. Multiphase Flow 23, 1063–1083.

Harmathy, T.Z., 1960. Velocity of large drops and bubbles in media of infinite or restricted extent. AIChE J. 6, 281–288.

Herbine, G.S., Perez-Blanco, H., 1995. Model of ammonia–water bubble absorber. ASHRAE Trans. 101, 1324–1332.

Herold, K.E., Radermacher, R., Klein, S.A., 1996. Absorption Chillers and Heat Pumps. CRC Press, Boca Raton.

Jayanti, S., Hewitt, G.F., 1992. Prediction of the slug-to-churn flow transition in vertical two-phase flow. Int. J. Multiphase Flow 18, 847–860.

Mcquillan, K.W., Whalley, P.B., 1985. Flow patterns in vertical two-phase flow. Int. J. Multiphase Flow 11, 161–175.

Merrill, T.L., Perez-Blanco, H., 1997. Combined heat and mass transfer during bubble absorption in binary solutions. Int. J. Heat Mass Transfer 40, 589–603.

Merrill, T.L., Setoguchi, T., Perez-Blanco, H., 1998. Compact bubble absorber design. J. Enhanced Heat Transfer 5, 249–256.

Mishima, K., Ishii, I., 1984. Flow regime transition criteria for two-phase flow in vertical tubes. Int. J. Heat Mass Transfer 27, 726–734.

Nicklin, D.J., Wilkes, J.O., Davidson, J.F., 1962. Two-phase flow in vertical tubes. Trans. Inst. Chem. Engrs. 40, 61–68.

Sohn, B.H., Kim, B.J., 2000. Counter-current gas–liquid two-phase flow in a narrow rectangular channel. In: Proceedings of the 4th JSME–KSME Thermal Engineering Conference, vol. 1, pp. 729–734.

Taitel, Y., Barnea, D., 1983. Countercurrent gas–liquid vertical flow model for flow pattern and pressure drop. Int. J. Multiphase Flow 9, 637–647.

Usui, K., 1989. Vertical downward two-phase flow, (II) flow regime transition criteria. J. Nucl. Sci. Technol. 26, 1013–1022.

Wallis, G.B., 1969. One-dimensional Two-phase Flow. McGraw-Hill, New York.

Webb, R.L., 1994. Principles of Enhanced Heat Transfer. Wiley, New York.

Yamaguchi, K., Yamazaki, Y., 1982. Characteristics of counter-current gas–liquid two-phase flow in vertical tubes. J. Nucl. Sci. Technol. 19, 985–996.

Yamaguchi, K., Yamazaki, Y., 1984. Combinated flow pattern map for cocurrent and countercurrent air–water flows in vertical tubes. J. Nucl. Sci. Technol. 21, 321–327.